



Folding Kinetics of the Cooperatively Folded Subdomain of the I κ B α Ankyrin Repeat Domain

Ingrid DeVries¹, Diego U. Ferreiro^{2,3},
Ignacio E. Sánchez^{2,3} and Elizabeth A. Komives^{1*}

¹Department of Chemistry and Biochemistry, University of California, San Diego, 9500 Gilman Drive, La Jolla, CA 92093-0378, USA

²Protein Physiology Laboratory, Departamento de Química Biológica, Facultad de Ciencias Exactas y Naturales, Universidad de Buenos Aires, C1428EGA Buenos Aires, Argentina

³Consejo Nacional de Investigaciones Científicas y Técnicas de Argentina, C1428EGA Buenos Aires, Argentina

Received 17 December 2010;
received in revised form
3 February 2011;
accepted 9 February 2011

Edited by K. Kuwajima

Keywords:

protein folding;
repeat protein;
 ϕ value;
folding landscape;
NF κ B

The ankyrin repeat (AR) domain of I κ B α consists of a cooperative folding unit of roughly four ARs (AR1–AR4) and of two weakly folded repeats (AR5 and AR6). The kinetic folding mechanism of the cooperative subdomain, I κ B α _{67–206}, was analyzed using rapid mixing techniques. Despite its apparent architectural simplicity, I κ B α _{67–206} displays complex folding kinetics, with two sequential on-pathway high-energy intermediates. The effect of mutations to or away from the consensus sequences of ARs on folding behavior was analyzed, particularly the GXTPLHLA motif, which have not been examined in detail previously. Mutations toward the consensus generally resulted in an increase in folding stability, whereas mutations away from the consensus resulted in decreased overall stability. We determined the free energy change upon mutation for three sequential transition state ensembles along the folding route for 16 mutants. We show that folding initiates with the formation of the interface of the outer helices of AR3 and AR4, and then proceeds to consolidate structure in these repeats. Subsequently, AR1 and AR2 fold in a concerted way in a single kinetic step. We show that this mechanism is robust to the presence of AR5 and AR6 as they do not strongly affect the folding kinetics. Overall, the protein appears to fold on a rather smooth energy landscape, where the folding mechanism conforms a one-dimensional approximation. However, we note that the AR does not necessarily act as a single folding element.

© 2011 Elsevier Ltd. All rights reserved.

Introduction

I κ B α , an inhibitor of the transcription factor nuclear factor κ B (NF κ B), contains an ankyrin repeat domain (ARD) with six ankyrin repeats (ARs). I κ B α is bound to NF κ B in the cytoplasm, until extracel-

lular signals trigger ubiquitin-mediated proteasome-dependant degradation of the I κ B α ,¹ allowing NF κ B to enter the nucleus and up-regulate the transcription of a variety of target genes, among which is the gene for I κ B α .¹ Newly synthesized I κ B α then enters the nucleus and interferes with the NF κ B–DNA interaction, eventually returning the NF κ B to the cytoplasm and the cell to the resting state. It has been shown that I κ B α is only fully folded when bound to NF κ B; AR5 and AR6 of I κ B α are weakly folded in free I κ B α .^{2,3} Upon urea challenge, AR1 to AR4 unfold cooperatively, whereas AR5 and AR6 undergo a noncooperative transition.⁴

*Corresponding author. E-mail address:
ekomives@ucsd.edu.

Abbreviations used: NF κ B, nuclear factor κ B; I κ B α , inhibitor of NF κ B; AR, ankyrin repeat; ARD, ankyrin repeat domain; TSE, transition state ensemble.

The folding behavior of AR proteins is interesting because there are no long-range contacts, and stabilization is only through local interactions.⁵ ARs are composed of a β -hairpin, two anti-parallel α -helices (distinguished as “inner” or “helix 1” and “outer” or “helix 2”), and a variable loop. Each repeat makes contacts only within the repeat and with residues of adjacently stacked repeats. With contacts only a short sequence distance away, it has been proposed that the folding of ARDs is “one-dimensional.”⁶

The folding of several ARDs has been studied in detail. D34⁷ and the Notch⁸ ankyrin domain, with 12 and 7 ARs each, were analyzed by making a single mutation in an analogous position on each repeat. This type of analysis assumes the single position can represent the whole AR unit and thus allows direct comparison of the effect of each AR on folding of the ARD. In each Notch AR, the Ala at the start of helix 1 was mutated to Gly, and a comparison of the folding kinetics of these mutants showed that Notch folds through an on-pathway intermediate in which the three central ARs were structured.⁹ In each D34 AR, the valine and/or one of the two leucine residues in helix 2 was mutated, and a comparison of these mutants showed that folding involved a polarized intermediate, in which the C-terminal half of the protein was structured. However, mutation in the C-terminal ARs altered the intermediate and shifted the folding pathway.¹⁰

The folding kinetics of mutant ARDs were studied in p16^{INK4A} and myotrophin. In these studies, conservative mutations, generally removing a single methyl group from the side chain of the residue, were examined across the protein sequence to determine how interactions throughout the protein are formed along the folding pathway, allowing a classic ϕ -value analysis to be performed. The four-AR-containing protein p16^{INK4A} was found to unfold sequentially via a polarized transition state in which the two C-terminal ARs were structured but the two N-terminal ARs were not.¹¹ Similarly, myotrophin folds sequentially, with the C-terminal ARs initiating the folding reaction.¹² In each of these studies, mutations in a particular AR were considered as a group, with the goal of identifying which ARs were folded at the transition state of the folding pathway.

Additionally, the folding of p19^{INK4d}^{13,14} and tANK¹⁵ was studied with NMR complementing equilibrium and kinetic experiments to obtain residue-specific folding information. Both of these five-AR-containing proteins were found to have populated intermediates at equilibrium, with the three C-terminal ARs folded.

Several groups have published consensus sequences of the AR motif based on a bioinformatic analysis of the hundreds of available AR sequences.^{16–21} These sequences differ in the details, but share a core “minimum” consensus with two main regions: one region encompasses the hairpin and the beginning of

helix 1, and the second region covers the end of helix 2 and part of the variable loop (Fig. 1a).²⁴ In addition, the folding of full-consensus designed ARDs (DARPin) has been studied.^{18–20,25–27} Natural ARDs are generally marginally stable, but designed ARD proteins based on the consensus sequence have much higher thermal and chemical stability. Consensus ARDs also fold much faster and unfold much more slowly than naturally occurring ARDs of similar size.²⁶ Naturally occurring ARDs deviate substantially from the consensus: I κ B α matches the minimum consensus for just over 50% of residues. I κ B α and other large ARDs, such as the Notch ARD, conform more to the consensus in residues 4–12, while smaller ARD-containing proteins, such as p16 and myotrophin, conform better in residues 20–30. Guo *et al.* recently showed that the TPLH motif in the first region of the AR consensus is a major stabilizing factor in central repeats of AR proteins.²⁸ However, how the consensus residues confer stability on ARDs and why naturally occurring ARDs deviate so much from the consensus are still not well understood.

Here, we examined the folding kinetics of the first four repeats of I κ B α , I κ B α _{67–206}, the cooperative folding unit in the I κ B α ARD. I κ B α _{67–206} displays a complex folding behavior, indicative of the presence of on-pathway high-energy intermediates. We also performed mutational analysis, using the AR consensus as a guide to determine the effect of individual consensus positions on folding behavior. Our studies particularly focus on the consensus residues GXTPLHLA, which have not been examined in detail previously. Restoration of a consensus residue resulted in an increase in mutant stability, whereas mutation away from the consensus resulted in decreased stability. Additionally, we found that the majority of mutations affected the unfolding rate, while the only mutations found to affect the folding rate were located in the second helices of AR3 and AR4. By scanning the consensus, we were able to identify parts of a single AR that influence the folding and unfolding rates. We suggest that folding initiates by the formation of the interface of the outer helices of AR3 and AR4, which appears to be folded in the first transition state, while the remainder of the protein folds later. We also show that these conclusions carry over to the full six repeats of I κ B α as the presence of AR5 and AR6 does not seem to affect the folding pathway.

Results

Introduction of a tryptophan probe in the cooperatively folding part of I κ B α : I κ B α _{67–206} A133W

We previously showed that I κ B α _{67–206} has similar stability to I κ B α _{67–287}, but lacks the steep pre-

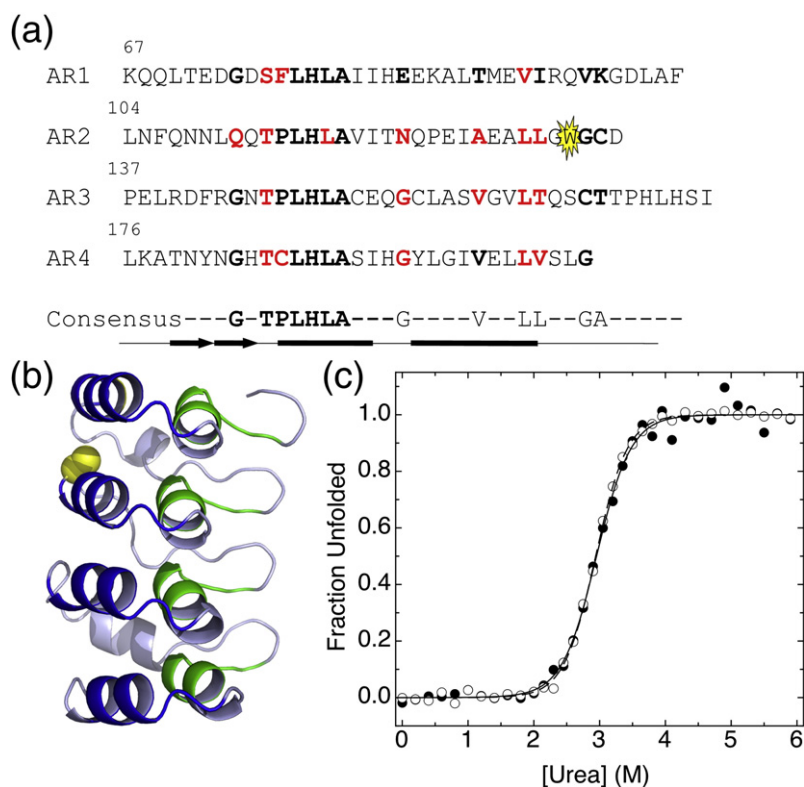


Fig. 1. (a) The IκBα₆₇₋₂₀₆W sequence with consensus positions in bold. Tryptophan reporter is highlighted in yellow. Mutated residues are shown in red. Secondary structure is shown below the sequence; the thick arrows represent a β-hairpin and the thick lines represent α-helices. The minimum consensus is represented below the sequence, with highly conserved residues shown and less conserved residues represented by dashes. (b) IκBα₆₇₋₂₀₆W structure, from NFκB/IκBα₇₀₋₂₈₇ structure (PDB: 1NF1).²² The backbone of the first consensus region encompassing the hairpin and the beginning of helix one is colored green, and the backbone of the second consensus region encompassing helix 2 and the first part of the variable loop is colored blue. A133 is highlighted in yellow. Modifications were performed in PyMol.²³ (c) Fraction unfolded from equilibrium urea denaturation of IκBα₆₇₋₂₀₆W (3 μM), monitored by the CD signal at 225 (filled circles) or fluorescence (open circles). Lines

are from global fits of equilibrium denaturation curves at several temperatures to a two-state model with shared m -values (CD m -value is 2.06 kcal mol⁻¹ M⁻¹; fluorescence m -value is 2.12 kcal mol⁻¹ M⁻¹).

transition baseline characteristic of the noncooperative transition attributed to AR5 and AR6 in IκBα₆₇₋₂₈₇.⁴ In order to probe just the cooperative folding transition, a deletion mutant of IκBα containing only the first four ARs, IκBα₆₇₋₂₀₆, was used. A tryptophan residue was engineered into AR2 (A133W) as a fluorescent reporter, as the only

natural tryptophan in IκBα is in AR6 (Fig. 1a, b). The four-AR fragment of the ARD of IκBα recapitulates the entire cooperatively folding unit of the full-length ARD. The A133W mutant, hereinafter referred to as IκBα₆₇₋₂₀₆W (Table 1), had the same stability as wild-type IκBα₆₇₋₂₀₆,⁴ and allowed unfolding to be monitored by both fluorescence

Table 1. Folding properties of wild-type IκBα₆₇₋₂₀₆W at different temperatures

Experiment:	Equilibrium ^a		Kinetics ^b				ΔG_{eq}^c
	Temperature (°C)	CD ΔG_{eq}	Fluorescence ΔG_{eq}	k_{12}	k_{21}	k_{32}	
5	6.3 ± 0.2	6.5 ± 0.1	1.5	1.7×10^4	48	0.41	5.9
10	6.1 ± 0.2	6.2 ± 0.1	2.2	1.9×10^4	63	0.74	5.7
15	5.8 ± 0.2	6.0 ± 0.1	2.9	0.80×10^4	37	1.6	6.3
20	5.7 ± 0.2	5.9 ± 0.1	3.5	0.56×10^4	42	3.2	6.3
25	5.9 ± 0.2	6.3 ± 0.1	6.2	0.68×10^4	61	5.9	6.0

Folding stabilities (ΔG_{eq}) are reported in kcal mol⁻¹, and rates in s⁻¹.

^a Equilibrium denaturation experiments were measured by CD or total fluorescence. All temperatures were globally fit to a two-state model with baseline drift with shared m -values of 2.06 kcal mol⁻¹ M⁻¹ for CD and 2.12 kcal mol⁻¹ M⁻¹ for fluorescence. Reported errors are fit errors from the global fit of all temperatures.

^b Kinetic experiments were measured by stop-flow fluorescence. All temperatures were globally fit to a four-state model with shared m -values (in kcal mol⁻¹ M⁻¹): $m_{12} = -0.15$, $m_{21} = 0.96$, $m_{32} = 0.87$, and $m_{43} = 0.11$; m_{23} and m_{34} were set to 0 kcal mol⁻¹ M⁻¹ and k_{23} and k_{34} were set to 1×10^5 s⁻¹. The equilibrium m -value calculated from the m -values for all rate constants is $m_{\text{eq}} = -m_{12} + m_{21} + m_{32} + m_{43} = 2.09$ kcal mol⁻¹ M⁻¹, in agreement with the equilibrium measurement. To determine the experimental error, three independent data sets for wild-type IκBα₆₇₋₂₀₆W at 10 °C were globally fit with shared m -values. Individual rates were determined for each data set; from these, the standard deviation (SD) in each rate was calculated as 14% for k_{12} , 22% for k_{21} , 22% for k_{32} , and 2.6% for k_{43} .

^c ΔG_{eq} was calculated from the individual rates: $\Delta G_{\text{eq}} = RT \ln[k_{43} \times k_{32} \times k_{21} / (k_{12} \times k_{23} \times k_{34})]$. The SD in ΔG_{eq} was calculated to be 5.7%, based on the propagation of the SDs of the rates.

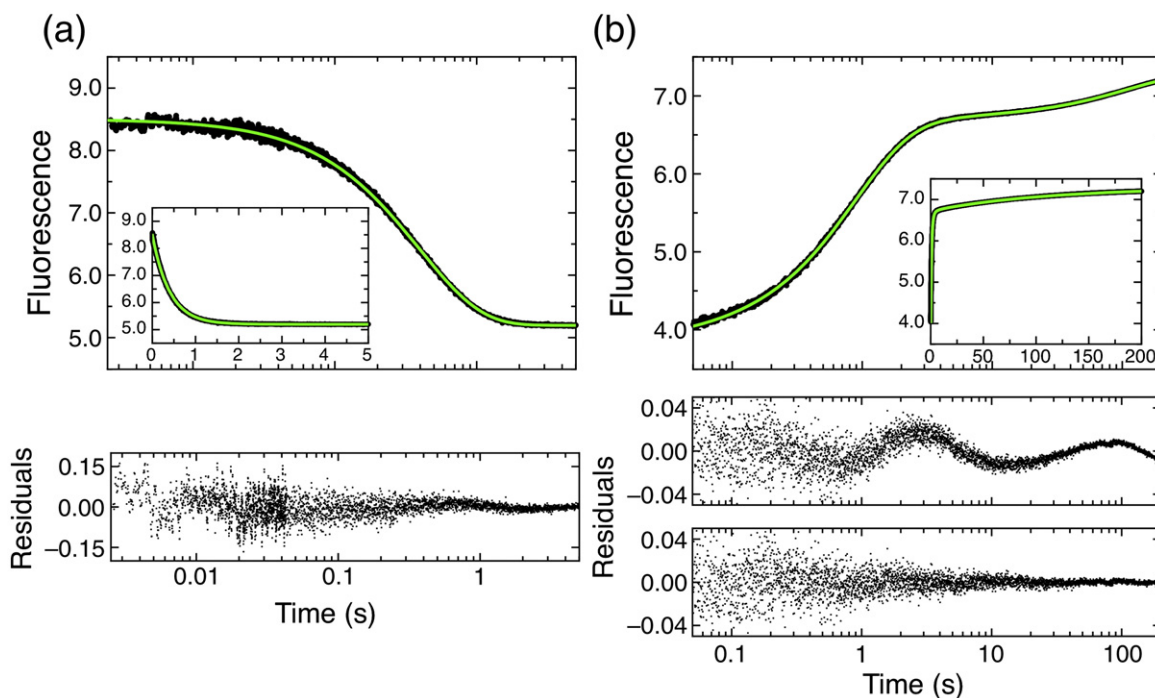


Fig. 2. Refolding and unfolding traces for IκBα₆₇₋₂₀₆W at 10 °C, monitored by total fluorescence. Insets show the same data with linear time scale. (a) Folded IκBα₆₇₋₂₀₆W was rapidly mixed to a final urea concentration of 6.5 M, and the change in fluorescence (of W133) was monitored (·). The unfolding trace was fit with a single exponential function (green line) with residuals shown below the plot. (b) IκBα₆₇₋₂₀₆W, unfolded in 4 M urea, was rapidly mixed to a final urea concentration of 0.7 M (·). The refolding trace was fit with triple exponential function (green line), with residuals for a double or triple exponential function shown below for comparison.

and circular dichroism (CD). For IκBα₆₇₋₂₀₆W, both fluorescence and CD equilibrium unfolding curves overlaid well and gave similar stabilities, demonstrating that both the local reporter (W133 in AR2) and the global reporter (CD monitoring helical structure) follow the same two-state cooperative transition (Fig. 1c).

IκBα₆₇₋₂₀₆W folding kinetics

The folding kinetics of IκBα₆₇₋₂₀₆W were measured by stopped-flow fluorescence at 10 °C. The decrease in fluorescence induced by unfolding of IκBα₆₇₋₂₀₆W by urea was fit to a single exponential because additional phases did not significantly improve the fit (Fig. 2a). Refolding experiments showed an increase in fluorescence induced by rapid mixing of denatured IκBα₆₇₋₂₀₆W with low concentrations of urea. Two to three exponential terms were required to fit the refolding curves (Fig. 2b), depending on the final denaturant concentration (see below). More importantly, the fluorescence change for both refolding and unfolding experiments has been fully accounted for, indicating that there are no additional kinetic phases taking place within the dead time of the instrument (Fig. 3a).

The observed unfolding and refolding rates from single mixing stopped-flow experiments were plot-

ted against urea concentration to yield a chevron plot (Fig. 3c). The plot reveals two distinct regions of unfolding distinguished by a significant change in slope near 5.5 M urea. The unfolding phase connects well with one of the refolding phases; this main refolding phase had the largest amplitude of the three refolding phases, accounting for 68–85% of the total amplitude (Fig. 3b). The main refolding phase showed a strong denaturant dependence. At low urea concentrations, a small downward curvature was observed in the chevron curve.

The slowest refolding phase had the second largest amplitude, accounting for approximately 18% of the total amplitude (Fig. 3b). This phase was relatively insensitive to denaturant concentration, with a rate of $9.3 \times 10^{-3} \text{ s}^{-1}$, up to urea concentrations of 2.5 M, beyond which the phase was not observed. Interrupted unfolding experiments show that this phase is due to a slow isomerization in the unfolded state (Supplementary Fig. S1). The rate constant for this refolding phase becomes faster in the presence of cyclophilin A, directly showing that the folding of these molecules is limited by Xaa-Pro peptide bond isomerization (Supplementary Fig. S2). IκBα₆₇₋₂₀₆W has five proline residues, all of which are in the *trans* conformation in the crystal structures.^{22,29} We conclude that the slowest refolding phase corresponds to isomerization-limited folding of unfolded

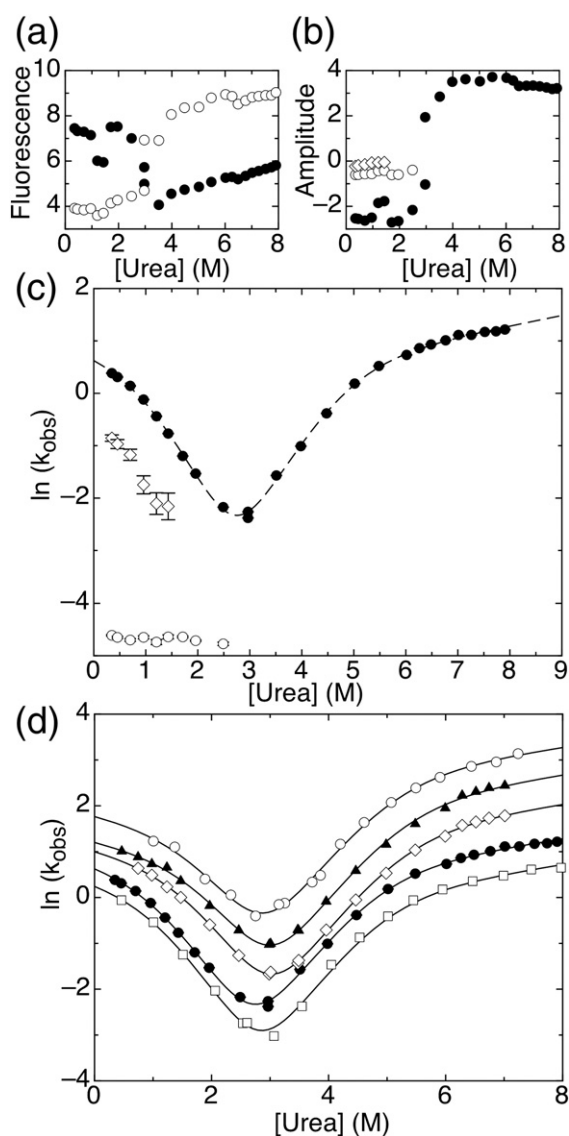


Fig. 3. Folding kinetics of IκBα₆₇₋₂₀₆W. (a) Starting (open circles) and ending (filled circles) fluorescence signals for refolding and unfolding traces. (b) Amplitudes of refolding and unfolding phases: unfolding and main refolding phase (filled circles), slow refolding phase (open circles), and intermediate refolding phase (open diamonds). (c) Effect of urea concentration on the observed folding or unfolding rate of IκBα₆₇₋₂₀₆W at 10 °C: unfolding and main refolding phase (filled circles), slow refolding phase (open circles), and intermediate refolding phase (open diamonds). Line shows the fit of the data collected at 10 °C from the global fit of several temperatures to a four-state model with shared m -values ($m_{12} = -0.15 \text{ kcal mol}^{-1} \text{ M}^{-1}$, $m_{21} = 0.96 \text{ kcal mol}^{-1} \text{ M}^{-1}$, $m_{32} = 0.87 \text{ kcal mol}^{-1} \text{ M}^{-1}$, and $m_{43} = 0.11 \text{ kcal mol}^{-1} \text{ M}^{-1}$; m_{23} and m_{34} were set to $0 \text{ kcal mol}^{-1} \text{ M}^{-1}$). (d) Main refolding and unfolding phases for IκBα₆₇₋₂₀₆W at 5 °C (open squares), 10 °C [filled circles; same as in (b) but shown for comparison], 15 °C (open diamonds), 20 °C (filled triangles), and 25 °C (open circles). Lines shown are from the global fit described in c.

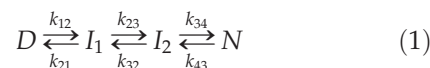
IκBα₆₇₋₂₀₆W molecules with one or more nonnative Xaa-Pro peptide bonds.³⁰

A third phase, intermediate in rate, had the smallest amplitude (Fig. 3b). This phase accounted for approximately 15% of the total amplitude at low urea concentrations, and its amplitude decreased gradually with increasing urea concentration until 2 M urea, where it was no longer observed. This phase showed denaturant sensitivity similar to the main phase. It should be noted that the uncertainty in the rates of this phase is high due to the small separation in rate from the main phase. Cyclophilin A shows little effect on the rate of this phase, suggesting that the reaction is not limited by proline isomerization; however, we were unable to obtain any further information on this phase due to its small amplitude. We speculate that this phase may be related to partial folding of IκBα₆₇₋₂₀₆W molecules with nonnative Xaa-Pro peptide bonds³⁰ or to isomerization of Xaa-NonPro peptide bonds in the unfolded state.³¹

Models to describe the folding kinetics of IκBα

The chevron plot formed by the single IκBα₆₇₋₂₀₆W unfolding phase and the main refolding phase (Fig. 3c) likely represents the main folding and unfolding event. Since there is a single relaxation, IκBα₆₇₋₂₀₆W folding is a two-state process without populated intermediates. However, the slight curvature at low urea concentrations and the significant change in slope at high urea concentrations suggest that the transition state region for IκBα₆₇₋₂₀₆W is complex.

Curved chevron plots can be explained by a broad transition state region.³² In this case, the curvature is described by a quadratic dependence of the free energies of activation on urea concentrations.^{33,34} This model could not describe the varying degrees of curvature in the chevron plot for IκBα₆₇₋₂₀₆W. A three-state folding model with an on-pathway high-energy intermediate,³⁵ which was used to describe the folding of the Notch ARD³³ and myotrophin mutants,¹² predicts a chevron with a kink only in the unfolding arm.³⁶ This model well described the data at high urea concentrations, but did not account for the curvature in the refolding arm of the chevron. A linear four-state model (Eq. 1) with two on-pathway, high-energy intermediates was required to fit the data.^{35,37}



In this model, the two intermediates are of higher free energy than both the unfolded and the folded state, and do not populate to a detectable amount. Fitting such a model to the data provides information about the relative free energies of the transition

state ensembles (TSEs) flanking the intermediates but not on the free energy of the intermediates themselves. To account for this, for data fitting, k_{23} and k_{34} were fixed to $1 \times 10^5 \text{ s}^{-1}$ and m_{23} and m_{34} were fixed at $0 \text{ kcal mol}^{-1} \text{ M}^{-1}$. The linear four-state model well describes the main folding reaction of IκBα_{67–206}W at 10 °C (Fig. 3c; Table 1).

Effect of temperature

The folding kinetics of IκBα_{67–206}W were examined at several temperatures. The observed refolding and unfolding rates increased across urea concentrations with temperatures from 5 °C to 25 °C while retaining similar slopes (Fig. 3d). As the temperature increased, the curvature observed in the refolding rates increased. The chevron plots at each temperature were globally fit using the four-state model with shared m -values (Fig. 3d). At all temperatures, the folding ΔG s calculated from the folding and unfolding rates agreed with the stabilities obtained from equilibrium experiments, which were separately globally fit to a two-state model (Table 1). Thus, the four-state model can describe the folding kinetics of IκBα_{67–206}W at different conditions. This result shows that the apparent changes of slope in the chevron plot are due to changes in the microscopic rate constants for an otherwise robust mechanism of IκBα_{67–206}W folding.

Consensus mutations

To probe the effect of sequence on the folding behavior of IκBα_{67–206}W, single mutations were made to consensus positions in the protein (Fig. 1a). Where the IκBα_{67–206}W sequence diverged from the consensus, the consensus was restored (e.g., Q111G); where the IκBα_{67–206}W sequence agreed with the consensus, conservative mutations were made (e.g., T113S). All mutants were expressed and purified, except L130V, G155A, and L202V, which could not be purified in the monomeric form; the stabilities and folding kinetics were then measured and compared to IκBα_{67–206}W. In total, 19 mutations were introduced, and of these, 16 yielded soluble protein that could be analyzed for folding kinetics and stability.

Initially, the stability of each mutant was determined by equilibrium urea denaturation, measured by CD or fluorescence (Table 2). As with IκBα_{67–206}W, there was good agreement between the two probes. This shows that the two-state mechanism for IκBα_{67–206}W equilibrium denaturation is robust to changes in sequence. Some mutants had considerable change in stability compared to IκBα_{67–206}W. V93L, Q111G, N122G, A127V, T164L, C186P, and V203L all had significantly higher stabilities than IκBα_{67–206}W, while T113S, L117V, L131V, T146S, L163V, T185S, and G194A had lower stabilities.

To further investigate the mutants, we performed stop-flow refolding and unfolding kinetic experiments to obtain chevron plots. It was possible to categorize the chevron plots into three different types (Fig. 4). Two mutants, both mutations being towards the consensus (S76T/F77P double mutant and V160A), did not differ significantly from wild type (Fig. 4a, j). The main phase of each chevron plot was globally fit with the four-state model using shared m -values (Fig. 4; Table 2). In the following sections, we compare the results with IκBα_{67–206}W (hereinafter referred to as WT) according to how each mutation affected the folding kinetics.

Only AR3 and AR4 mutations affected refolding kinetics

Of the 16 mutants analyzed, only 5 showed a more than 2-fold change in the k_{12} : L163V, T164L, T185S, G194A, and V203L (Table 2). L163V, a mutation away from the consensus in helix 2 of AR3, showed a decrease in k_{12} from 2.4 s^{-1} for the WT protein to 0.65 s^{-1} , and was destabilized by $0.78 \text{ kcal mol}^{-1}$ (Fig. 4k). Restoring the consensus, T164L also showed a strong effect by increasing k_{12} to 9.7 s^{-1} . This mutation stabilized the protein by $1.4 \text{ kcal mol}^{-1}$ (Fig. 4l).

In AR4, the T185S mutation away from the consensus increased k_{12} to 4.0 s^{-1} as well as the unfolding rates, but did not show an overall effect on ΔG . The G194A mutation, between helices 1 and 2, slowed refolding, decreasing k_{12} to 1.0 s^{-1} , and destabilized the protein by $0.6 \text{ kcal mol}^{-1}$ (Fig. 4o). Finally, the V203L mutation, restoring the consensus in helix 2 of AR4, increased k_{12} to 4.0 s^{-1} without affecting the overall unfolding rate, resulting in a stabilization of $1.5 \text{ kcal mol}^{-1}$ (Fig. 4p).

Most mutations had altered unfolding kinetics

The majority of mutations mainly caused changes in the unfolding rates (Fig. 4; Table 2). Three mutations, V93L (Fig. 4b), Q111G (Fig. 4c), and C186P (Fig. 4n), all towards the consensus, unfolded more slowly than WT; fits of the chevron plots also showed slower unfolding rates (k_{21} , k_{32} , and k_{43}) than WT, resulting in stabilization of the proteins by 1.8, 2.2, and $0.6 \text{ kcal mol}^{-1}$ respectively. Two additional mutations, N122G (Fig. 4f) and A127V (Fig. 4g), slowed k_{21} and k_{32} , but not k_{43} . Both these mutants were also stabilized by $0.9 \text{ kcal mol}^{-1}$.

Faster unfolding rates were observed for five mutants: T113S (Fig. 4d), L117V (Fig. 4e), L131V (Fig. 4h), T146S (Fig. 4i), and T185S (Fig. 4m), all mutations away from the consensus. Of these mutations, all but T185S increased k_{43} and k_{32} , and they destabilized the protein by 0.2, 0.5, 0.4, and 0.8, respectively. The T185S mutation decreased k_{32} but

Table 2. Folding properties of IκBα mutants

Experiment: Mutant	Equilibrium ^a		Kinetics ^b					Figure
	CD ΔG _{eq}	Fluorescence ΔG _{eq}	k ₁₂	k ₂₁	k ₃₂	k ₄₃	ΔG _{eq} ^c	
<i>IκBα₆₇₋₂₀₆W mutants</i>								
IκBα ₆₇₋₂₀₆ W	6.5±0.2	6.9±0.1	2.4	2.4 × 10 ⁴	57	0.71	5.7	4, dashed line
S76T/F77P	6.9±0.2	7.5±0.1	3.0	2.1 × 10 ⁴	51	0.55	6.1	4a
V93L	8.6±0.2	9.1±0.1	2.0	0.91 × 10 ⁴	13	0.25	7.5	4b
Q111G	8.4±0.2	9.2±0.1	3.7	2.0 × 10 ⁴	4.7	0.30	7.9	4c
T113S	5.6±0.2	6.1±0.1	2.1	1.3 × 10 ⁴	68	1.3	5.5	4d
L117V	5.5±0.2	5.8±0.1	2.2	1.4 × 10 ⁴	89	1.7	5.2	4e
N122G	7.5±0.2	8.2±0.1	2.7	1.5 × 10 ⁴	20	0.78	6.6	4f
A127V	6.8±0.2	7.3±0.1	1.8	0.79 × 10 ⁴	12	1.5	6.6	4g
L131V	4.7±0.2	5.0±0.1	2.6	2.0 × 10 ⁴	186	1.1	4.9	4h
T146S	4.9±0.2	5.3±0.1	2.3	1.6 × 10 ⁴	123	0.93	5.3	4i
V160A	6.7±0.2	7.2±0.1	2.7	1.8 × 10 ⁴	39	0.75	6.1	4j
L163V	5.2±0.2	5.6±0.1	0.65	1.7 × 10 ⁴	114	0.55	4.9	4k
T164L	7.3±0.2	7.8±0.1	9.7	0.76 × 10 ⁴	75	0.61	7.1	4l
T185S	5.7±0.2	6.1±0.1	4.0	4.3 × 10 ⁴	42	1.0	5.6	4m
C186P	7.2±0.2	7.7±0.1	2.1	1.6 × 10 ⁴	28	0.67	6.3	4n
G194A	5.4±0.2	5.8±0.1	1.0	3.1 × 10 ⁴	38	0.98	5.1	4o
V203L	7.3±0.2	7.8±0.1	4.0	0.50 × 10 ⁴	33	0.72	7.2	4p
<i>IκBα₆₇₋₂₈₇W mutants</i>								
IκBα ₆₇₋₂₈₇ W	7.1±0.2	7.4±0.3	0.48	1.3 × 10 ³	25	0.37	7.1	5▲
W258F	7.2±0.3	7.4±0.3	0.97	4.0 × 10 ³	30	0.36	6.8	5●
Q111G	8.7±0.3	9.2±0.3	0.55	0.94 × 10 ³	2.4	0.18	9.1	6b
T164L	7.5±0.3	7.5±0.3	1.8	0.47 × 10 ³	139	28	7.6	6d
V203L	7.4±0.3	7.4±0.3	0.70	0.88 × 10 ³	38	0.35	7.3	6f

Folding stabilities (ΔG_{eq}) are reported in kcal mol⁻¹, and rates in s⁻¹.

^a Equilibrium denaturation experiments measured by CD or total fluorescence. All IκBα₆₇₋₂₀₆W mutants were globally fit to a two-state model with baseline drift with shared *m*-values of 2.19 kcal mol⁻¹ M⁻¹ for CD and 2.35 kcal mol⁻¹ M⁻¹ for fluorescence. IκBα₆₇₋₂₈₇W mutants were also globally fit with shared *m*-values of 2.13 kcal mol⁻¹ M⁻¹ for CD and 2.20 kcal mol⁻¹ M⁻¹ for fluorescence. Reported errors are fit errors from the global fit of all mutants.

^b Kinetic experiments were measured by stop-flow fluorescence. All IκBα₆₇₋₂₀₆W mutants were globally fit to a four-state model with shared *m*-values (in kcal mol⁻¹ M⁻¹): *m*₁₂ = -0.11, *m*₂₁ = 0.98, *m*₃₂ = 0.89, and *m*₄₃ = 0.11; IκBα₆₇₋₂₈₇W mutants were similarly globally fit to a four-state model with shared *m*-values (in kcal mol⁻¹ M⁻¹): *m*₁₂ = -0.15, *m*₂₁ = 0.96, *m*₃₂ = 0.87, and *m*₄₃ = 0.11. For both, *m*₂₃ and *m*₃₄ were set to 0 kcal mol⁻¹ M⁻¹ and *k*₂₃ and *k*₃₄ were set to 1 × 10⁵ s⁻¹. The equilibrium *m*-value calculated from the *m*-values for all rate constants is *m*_{eq} = -*m*₁₂ + *m*₂₁ + *m*₃₂ + *m*₄₃ = 2.10 kcal mol⁻¹ M⁻¹ for IκBα₆₇₋₂₀₆W mutants and 2.09 kcal mol⁻¹ M⁻¹ for IκBα₆₇₋₂₈₇W mutants, both in agreement with the equilibrium measurement. To determine the experimental error, three independent data sets for wild-type IκBα₆₇₋₂₀₆W at 10 °C were globally fit with shared *m*-values. Individual rates were determined for each data set; from these, the SD in each rate was calculated as 14% for *k*₁₂, 22% for *k*₂₁, 22% for *k*₃₂, and 2.6% for *k*₄₃.

^c ΔG_{eq} was calculated from the individual rates: ΔG_{eq} = RT ln[k₄₃ × *k*₃₂ × *k*₂₁ / (*k*₁₂ × *k*₂₃ × *k*₃₄)]. The SD in ΔG_{eq} was calculated to be 5.7%, based on propagation of the SDs of the rates.

increased *k*₄₃ as well as the refolding rate, resulting in no overall change in stability.

Folding of the 6AR protein and mutants

We previously showed that the naturally occurring W258 in AR6 does not follow the cooperative unfolding transition, and we speculated that AR5 and AR6 do not contribute to the cooperative folding of IκBα₆₇₋₂₈₇ (the full 6ARs).⁴ To directly test this speculation, we introduced an A133W mutation into IκBα₆₇₋₂₈₇ and silenced W258: IκBα₆₇₋₂₈₇ A133W/W258F. This construct allowed direct comparison of the behavior of A133W fluorescence within the four-AR and six-AR constructs. Since IκBα₆₇₋₂₈₇ is more aggregation prone than its four-AR counterpart, we choose to perform these experiments at a lowered temperature of 5 °C. Experiments were performed at several concentra-

tions from 1 to 3 μM IκBα₆₇₋₂₈₇, and no concentration dependence of the folding kinetics was observed. Unfolding experiments with IκBα₆₇₋₂₈₇ A133W, which still contains W258, and the single tryptophan-containing IκBα₆₇₋₂₈₇ A133W/W258F revealed one or two folding phases, while refolding experiments showed two to four phases, similar to the four-AR protein. Despite the difference in rates, the chevron plots for both six-AR-containing proteins were remarkably similar to that for the four-AR-containing IκBα₆₇₋₂₀₆ A133W (Fig. 5; Table 2). We introduced three mutations studied in the 4AR protein to determine if the mutations would have the same effect in the 6AR protein (Table 2). We chose mutants with a large stabilizing effect on the 4AR protein Q111G, which decreased the unfolding rate (Fig. 6a and b); T164L, which increased the refolding rate (Fig. 6c and d); and V203L, which also increased the refolding rate (Fig. 6e and f). These

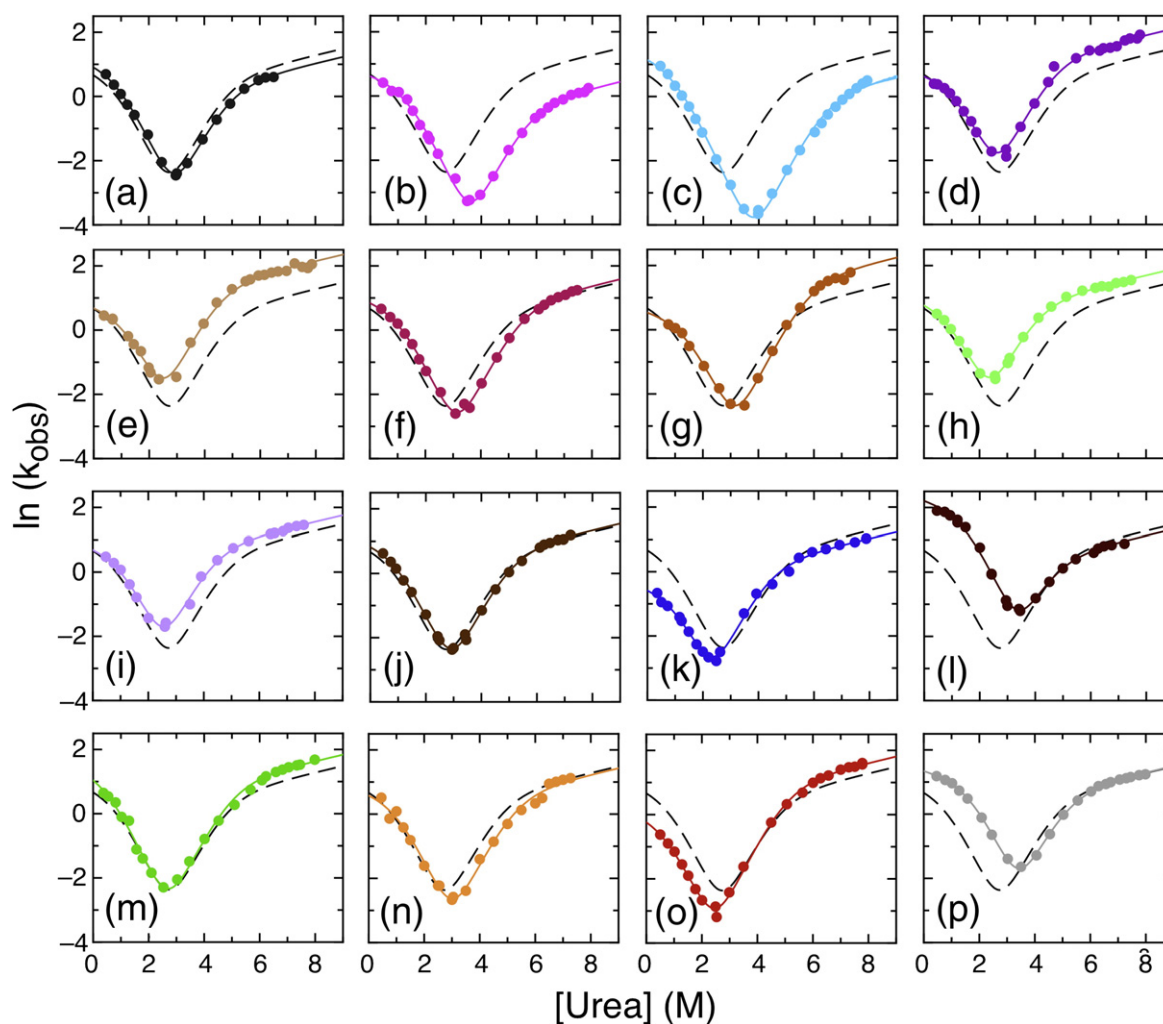


Fig. 4. Chevron plots for IκBα₆₇₋₂₀₆W mutants showing observed unfolding and major refolding rates at 10 °C. Lines shown are from the global fit of WT IκBα₆₇₋₂₀₆W and all mutants to the four-state model with shared m -values ($m_{12} = -0.11 \text{ kcal mol}^{-1} \text{ M}^{-1}$, $m_{21} = 0.98 \text{ kcal mol}^{-1} \text{ M}^{-1}$, $m_{32} = 0.89 \text{ kcal mol}^{-1} \text{ M}^{-1}$, and $m_{43} = 0.11 \text{ kcal mol}^{-1} \text{ M}^{-1}$; m_{23} and m_{34} were set to $0 \text{ kcal mol}^{-1} \text{ M}^{-1}$). The WT IκBα₆₇₋₂₀₆W fit is shown in all plots for comparison (black dashed line). The mutants shown are (a) S76T/F77P (dark grey), (b) V93L (pink), (c) Q111G (cyan), (d) T113S (dark purple), (e) L117V (tan), (f) N122G (magenta), (g) A127V (brown), (h) L131V (light green), (i) T146S (light purple), (j) V160A (brown), (k) L163V (blue), (l) T164L (dark red), (m) T185S (green), (n) C186P (orange), (o) G194A (red), and (p) V203L (light grey).

mutations in the 6AR context showed similar effects as had been seen in the 4AR context, again suggesting that the presence of AR5 and AR6 does not strongly affect the main folding route of the full-length ARD. The effects of the Q111G and T164L mutations were quantitatively similar in the four-AR and six-AR contexts, but the effect of the V203L mutation was less in the six-AR context. This result is most likely due to the proximity of the V203L mutation to the additional repeats.

Discussion

IκBα₆₇₋₂₀₆W shows a simple, two-state mechanism for equilibrium denaturation that yet has

complex folding kinetics; the chevron plot was nonlinear at both low and high urea concentrations, inconsistent with a simple two-state folding model. Simple folding models that may account for nonlinearity, including a two-state model with broad TSE and a three-state model with a metastable intermediate, proved insufficient. On the other hand, a four-state model with two high-energy intermediates fully accounted for the chevron plots of the wild-type IκBα₆₇₋₂₀₆W at all tested temperatures and the chevron plots for all mutants. In addition, folding ΔG values obtained from the global fitting of all the mutant equilibrium unfolding curves to a two-state model and those obtained from the global fitting of all the kinetic data agreed well.

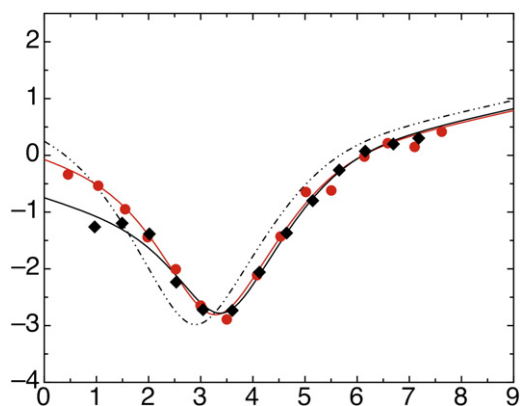


Fig. 5. Chevron plots for IκBα₆₇₋₂₈₇ A133W/W258F (red circles) and A133W (black triangles) showing main unfolding and refolding rates at 5 °C. Continuous lines show global fits of all six-AR mutants to a four-state model with shared m -values ($m_{12} = -0.15 \text{ kcal mol}^{-1} \text{ M}^{-1}$, $m_{21} = 0.96 \text{ kcal mol}^{-1} \text{ M}^{-1}$, $m_{32} = 0.87 \text{ kcal mol}^{-1} \text{ M}^{-1}$, and $m_{43} = 0.11 \text{ kcal mol}^{-1} \text{ M}^{-1}$; m_{23} and m_{34} were set to 0 $\text{kcal mol}^{-1} \text{ M}^{-1}$). For comparison, the fit of four-AR IκBα₆₇₋₂₀₆W (main phase at 5 °C) to the four-state model is shown as a dashed line.

Consensus stabilization

The folding kinetics of 16 mutants of IκBα₆₇₋₂₀₆W were analyzed and compared; of these, eight conservative mutations were made at positions conforming to the consensus (T113S, L117V, L131V, T146S, V160A, L163V, T185S, and G194A), and all except V160A and T185S destabilized IκBα₆₇₋₂₀₆W. Eight mutations (S75T/F77P, V93L, Q111G, N122G, A127V, T164L, C186P, and V203L) restored the consensus at positions not in agreement with the consensus; all of these stabilized IκBα₆₇₋₂₀₆W. Previous studies on IκBα₆₇₋₂₈₇, a longer construct containing all six ARs of IκBα, also reported that Q111G and C186P stabilized.⁴ These results suggest a strong correlation between the ankyrin consensus and the folding stability of IκBα₆₇₋₂₀₆W. For every mutation that changed the folding stability of IκBα₆₇₋₂₀₆W, the construct with the consensus residue was always more stable. This result is consistent with the observation that full consensus AR proteins have very high stabilities.^{18,25,26} Although it was known that full consensus proteins are more stable, a comprehensive analysis of every consensus position has not been

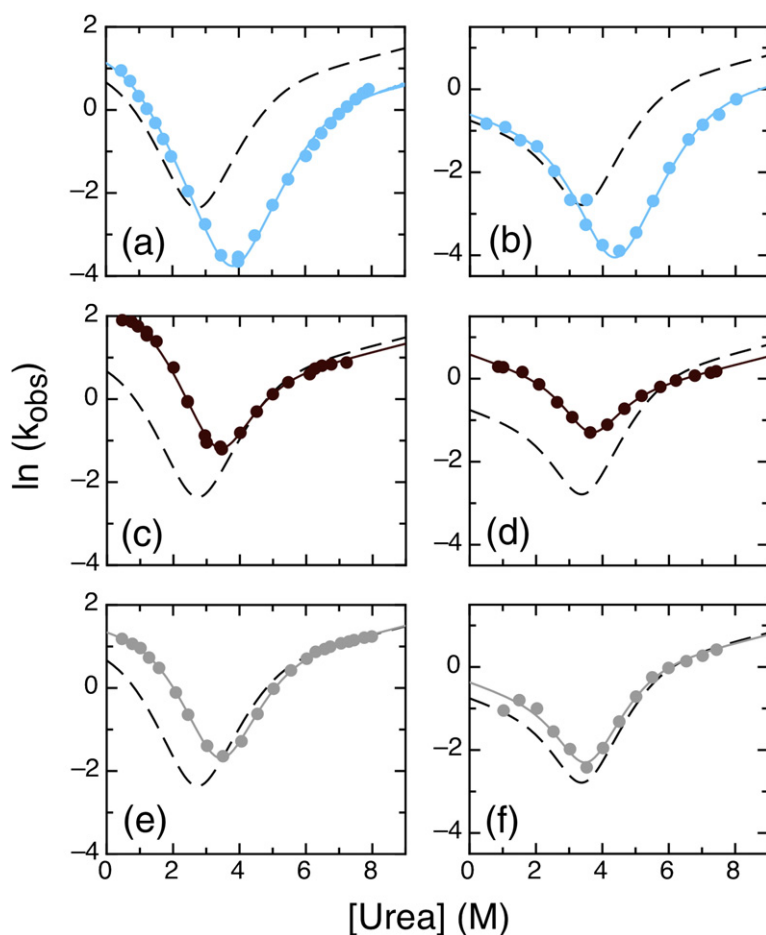


Fig. 6. Chevron plots for IκBα A133W mutants showing observed unfolding and refolding rates at 5 °C (six-AR) and 10 °C (four-AR). (a) Four-AR IκBα₆₇₋₂₀₆ A133W Q111G; (b) six-AR IκBα₆₇₋₂₈₇ A133W Q111G; (c) four-AR IκBα₆₇₋₂₀₆ A133W T164L; (d) six-AR IκBα₆₇₋₂₈₇ A133W T164L; (e) four-AR IκBα₆₇₋₂₀₆ A133W V203L; (f) six-AR IκBα₆₇₋₂₈₇ A133W V203L. Lines show global fits of all four-AR or six-AR mutants to a four-state model with shared m -values (as described in Figs. 4 and 5) of WT (dashed line) and mutants (continuous lines). The color scheme for the individual mutations is the same as that used in Fig. 4.

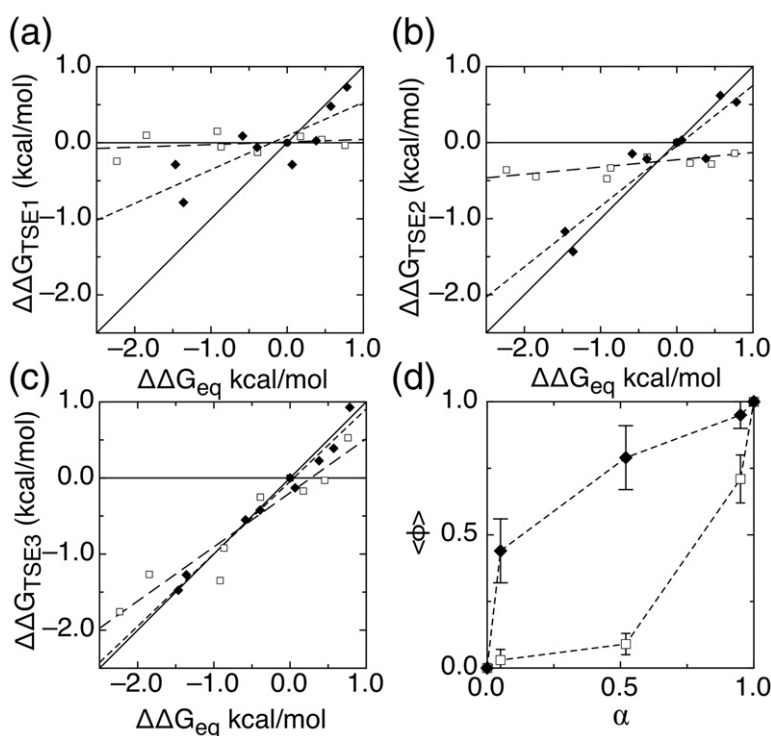


Fig. 7. Leffler plots of $\Delta\Delta G_{TSE}$ compared to the $\Delta\Delta G_{eq}$ of IκBα₆₇₋₂₀₆W mutants for (a) TSE1, (b) TSE2, and (c) TSE3. AR1 and AR2 mutants (open squares) are shown with linear fits of these mutants (long-dashed lines), with slopes of 0.03, 0.07, and 0.70 corresponding to the average ϕ -values for AR1 and AR2 mutants in the three TSEs. AR3 and AR4 mutants (filled diamonds) are shown with linear fits of these mutants (short-dashed lines), with slopes of 0.45, 0.79, and 0.95 corresponding to average ϕ -values for AR3 and AR4 mutants in the three TSEs. For reference, continuous lines of slopes 0 and 1 are shown, corresponding to average ϕ -values of 0 and 1. (d) Average ϕ -value versus α , the location of each TSE along the reaction coordinate, for AR1 and AR2 mutants

(filled circles) and AR3 and AR4 mutants (open circles). α was calculated globally as 0.05, 0.52, and 0.95 for IκBα₆₇₋₂₀₆W and 0.07, 0.35, and 0.95 for IκBα₆₇₋₂₈₇W from the kinetic m -values using the following equations:

$$\begin{aligned}\alpha_{TSE1} &= -m_{12}/m_{eq} \\ \alpha_{TSE2} &= (-m_{12} + m_{21})/m_{eq} \\ \alpha_{TSE3} &= (-m_{12} + m_{21} + m_{34})/m_{eq}\end{aligned}$$

studied. The stability of the full consensus protein could have been because one or two of the consensus amino acids were responsible for stability, while the others had some other function. Here, we specifically probed the consensus positions, and our results show that each and every consensus position, one at a time, imparts stability. Furthermore, the results show that the consensus residues have differential effects on folding kinetics depending on their location within a single repeat.

Effect of mutations on folding

The effect of mutations on the folding and unfolding rates of IκBα₆₇₋₂₀₆W can be used to develop a picture of the folding pathway. Phi-value analysis is a useful tool for analyzing the change in folding rate upon mutation as compared with the change in stability³⁸:

$$\Delta\Delta G_{TSE} = \frac{RT \ln k_f^{WT}}{RT \ln k_f^{mut}}, \quad \Phi = \frac{\Delta\Delta G_{TSE}}{\Delta\Delta G_{eq}}$$

Mutants that change the stability of the protein but do not affect the folding rate have a Φ_F value of 0, suggesting that the contacts to this residue are not

formed yet in the transition state. Conversely, mutants that change the stability of the protein solely because of a change in folding rate have a Φ_F value of 1. Applying ϕ -value analysis to a set of mutations throughout a protein can give structural information about the transition state for folding and can show which regions or structural features fold first.

Phi-value analysis on a more complex folding pathway such as the one we observed for IκBα₆₇₋₂₀₆W can also be performed on the individual TSEs in the folding reaction. The folding rate to each TSE was calculated and used to determine the $\Delta\Delta G$ for each TSE. To determine the average degree of folding in each TSE, we performed a Leffler analysis on the $\Delta\Delta G$ s of each TSE (Fig. 7; Table 3).^{38,39} We found it useful to plot the $\Delta\Delta G$ values for residues in AR3 and AR4 separately from those in AR1 and AR2 and to fit each separately. The results revealed that the slope of the Leffler plot for AR1 and AR2 was near zero for TSE1 and TSE2, corresponding to an average ϕ -value close to zero. On the other hand, the slope for AR3 and AR4 was 0.45 for TSE1 and 0.79 for TSE2, indicating a progressive folding of this region along the reaction coordinate. This differentiation between the N- and C-terminal repeats is made more apparent

Table 3. Folding landscape of IκBα₆₇₋₂₀₆W mutants

Mutant	$\Delta\Delta G_{\text{eq}}^a$	$\Delta\Delta G_{\text{TSE1}}$	$\Delta\Delta G_{\text{TSE2}}$	$\Delta\Delta G_{\text{TSE3}}$	Φ_{TSE1}	Φ_{TSE1}	Φ_{TSE1}
<i>A. IκBα₆₇₋₂₀₆W mutants</i>							
S76T/F77P	-0.4	-0.13	-0.19		-0.25	n/a ^b	
V93L	-1.8	0.10	-0.45	-1.27	-0.05	0.24	0.69
Q111G	-2.2	-0.24	-0.36	-1.76	0.11	0.16	0.79
T113S	0.2	0.08	-0.27	-0.17	n/a		
L117V	0.5	0.04	-0.28	-0.03	n/a		
N122G	-0.9	-0.05	-0.33	-0.92	0.06	0.38	1.06
A127V	-0.9	0.15	-0.48	-1.35	-0.16	0.52	1.47
L131V	0.8	-0.03	-0.14	0.53	-0.04	-0.18	0.69
T146S	0.4	0.03	-0.21	0.23	n/a		
V160A	-0.4	-0.06	-0.22	-0.42	n/a		
L163V	0.8	0.73	0.53	0.93	0.93	0.68	1.18
T164L	-1.4	-0.79	-1.43	-1.27	0.58	1.05	0.94
T185S	0.1	-0.29	0.03	-0.13	n/a		
C186P	-0.6	0.09	-0.15	-0.55	-0.15	0.25	0.94
G194A	0.6	0.48	0.62	0.39	0.84	1.08	0.68
V203L	-1.5	-0.29	-1.17	-1.48	0.20	0.80	1.01
<i>B. IκBα₆₇₋₂₈₇W mutants</i>							
Q111G	-2.0	-0.08	-0.25	-1.56	0.04	0.13	0.80
T164L	-0.5	-0.73	-1.29	-0.34	1.46	2.57	0.69
V203L	-0.2	-0.21	-0.42	-0.19	n/a ^b		

^a $\Delta\Delta G$ s were calculated in comparison to WT IκBα₆₇₋₂₀₆W or IκBα₆₇₋₂₈₇W, using data from the kinetic experiments. Φ -values were calculated as $\Delta\Delta G_{\text{TSE}}/\Delta\Delta G_{\text{eq}}$.

^b Phi-values were not calculated for mutants with $\Delta\Delta G_{\text{eq}} < 0.5$.

by plotting the average ϕ -value for each group against the degree of compaction along the reaction coordinate, α (Fig. 7d). AR3 and AR4 again show a folded character much earlier than AR1 and AR2, which are not folded until the folding reaction is nearly complete. This result recapitulates previous ϕ -value analyses on other four-AR-containing proteins, p16¹¹ and myotrophin.¹² For p16, the majority of mutants have high ϕ -values; only a few mutants, clustered on AR1 and AR2, have ϕ -values near zero. Myotrophin showed a similarly C-terminally polarized transition state.

To uncover more details, a residue-specific ϕ -value analysis was performed on each of the TSEs for the IκBα₆₇₋₂₀₆W mutants that had an overall $\Delta\Delta G_{\text{eq}} > 0.5$ kcal mol⁻¹ (Table 3). The ϕ -values revealed that residues L163, T164, and G194 had high ϕ -values in TSE1 (Fig. 8a). These residues are all located in helix 2 (L163 and T164 in AR3, and G194 in helix 4). Thus, folding appears to initiate with only the interaction between the outer helices of AR3 and AR4. Although myotrophin, p16, and IκBα₆₇₋₂₀₆W all have similar transition states with parts or all of the two C-terminal repeats folded, IκBα₆₇₋₂₀₆W appears to have a much smaller folded region, at least in the first TSE, with only the outer helices of AR3 and AR4 folded.

Moderate ϕ -values for N122 and A127 indicate that helix 2 in AR2 of IκBα₆₇₋₂₀₆W folds in TSE2 (Fig. 8b). Consistent with the Leffler analysis, it is not until TSE3, which is 95% as compact as the native state, that residues within helix 1 and the β -hairpins (Q111 and C186) appear to fold (Fig. 8c). In

fact, the C186P mutation in AR4 only has a ϕ -value near 1 in TSE3, indicating that all of AR4 is not folded at once. Indeed, the results presented here suggest that the two parts of the consensus represent different folding/stacking nuclei and that the outer helices (helix 2 of each repeat) fold/stack early in the folding pathway, whereas the inner helices (helix 1) and β -hairpins fold/stack later. It is possible, then, that as was suggested in our earlier theoretical work,⁶ a single AR does not represent a single foldon and that further refinements of a general ARD folding mechanism will be required, in which other elements are treated as foldons rather than whole ARs.

Comparison of the 4AR and 6AR proteins

We had previously shown via equilibrium experiments that AR5 and AR6 did not appear to contribute to the equilibrium stability of IκBα. Here, we showed for three separate cases that mutations in the cooperative folding 4AR unit had the same effect in the full 6AR context. These results strongly suggest that AR5 and AR6 not only do not contribute to equilibrium stability but also do not affect to the folding pathway of the cooperatively folding part of the IκBα ARD. This is in contrast to many other studies in which adding ARs to a cooperatively folding ARD enhances stability and sometimes alters the folding pathway.^{14,21,40} These results again highlight that the AR5-AR6 region of IκBα is weakly folded and will perhaps have unique characteristics as

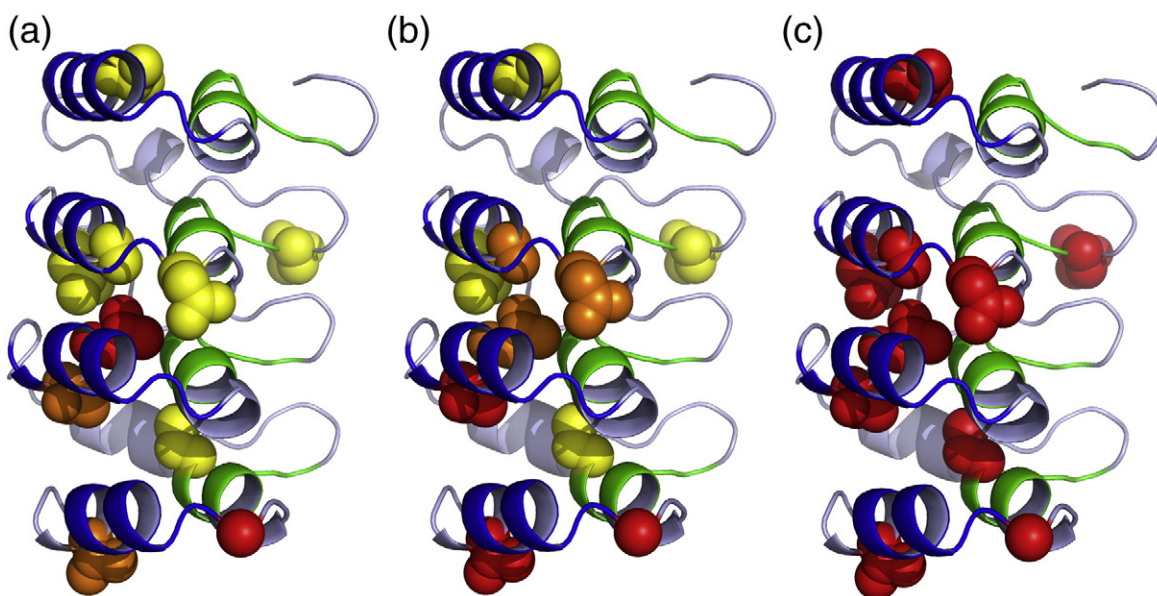


Fig. 8. Phi-values for (a) TSE1, (b) TSE2, and (c) TSE3 are plotted on the structure of IκBα₆₇₋₂₀₆W. The backbone of the protein is colored as in Fig. 1. Mutated residues are shown in spheres and colored by Φ-value, with yellow for below 0.3, orange for 0.3 to 0.6, and red for >0.6; modifications were performed in PyMol.²³

compared to repeats in other well-studied ARD-containing proteins.

Materials and Methods

Expression/purification

IκBα mutations were introduced using QuikChange mutagenesis.⁴¹ Human IκBα constructs were expressed and purified as described previously.⁴² The final purification step was on a Superdex-75 gel filtration column (GE Healthcare). The proteins were stored at 4 °C and used within 1 week of gel filtration. Protein concentrations were determined by spectrophotometry, using extinction coefficients of 2980 M⁻¹ cm⁻¹ for IκBα₆₇₋₂₀₆, 8480 M⁻¹ cm⁻¹ for IκBα₆₇₋₂₀₆W and mutants, 12950 M⁻¹ cm⁻¹ for IκBα₆₇₋₂₈₇ with a single tryptophan, and 18450 M⁻¹ cm⁻¹ for IκBα₆₇₋₂₈₇ with two tryptophans.

Urea preparation

Urea (Fisher Scientific, Pittsburg, PA, USA) was dissolved in water and then treated with AG 501-X8 (D) resin (BioRad Laboratories, Hercules, CA, USA) for 1 h to remove cyanate contaminants.⁴³ Resin was filtered out with a 0.2-μm filter, and buffer salts were added to the purified urea. Urea concentrations were checked by refractometry.⁴⁴ Urea was used within 2 days of resin treatment to prevent reaccumulation to cyanate.

Equilibrium folding experiments

Equilibrium folding experiments were performed with an Aviv 202 spectropolarimeter (Aviv Biomedical, Lakewood, NJ, USA) with a Hamilton Microlab 500 titrator

(Hamilton, Reno, NV, USA). A 1-cm fluorescence quartz cuvette containing 2.0 ml of 1–4 μM of the native protein in buffer [10 mM NaHPO₄, 50 mM NaCl, 1 mM DTT, 0.5 mM EDTA (ethylenediamine tetraacetic acid), pH 7.5] was titrated with denatured protein (7.3–8.4 M urea in buffer) in 30 to 40 injection steps. After each injection, samples were equilibrated with constant stirring at 70–80 rpm for 180 s prior to data collection. The CD signal was collected at 225 nm, averaged over 5 to 10 s, and the fluorescence signal was collected through a 320-nm cutoff filter with an excitation wavelength of 280 nm, averaged over 2 to 5 s. Experiments were performed at 10 °C unless otherwise stated.

Equilibrium folding curves were fit to a two-state folding model, assuming a linear dependence of the folding free energy on denaturant concentration.⁴⁴ The pre-transition (native) and post-transition (unfolded) baselines were treated as linearly dependent on denaturant concentration. The data were globally fit to

$$S_{\text{obs}} = (a_1 + p_1[\text{Urea}]) + (a_2 + p_2[\text{Urea}])\exp(-(\Delta G - m[\text{Urea}] / RT)) / (1 + \exp(-(\Delta G - m[\text{Urea}] / RT)))$$

where S_{obs} is the observed signal; p_1 and p_2 are the pre- and post-transition baselines, with a_1 and a_2 as their corresponding y -intercepts; ΔG is the folding free energy in water; and m is the cooperativity parameter (m -value). The data were fit using a nonlinear least square fitting algorithm in Kaleidagraph (Synergy Software, Reading, PA, USA) or Profit (QuantumSoft, Uetikon am See, Switzerland).

Folding kinetics

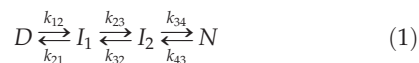
Kinetic folding experiments were performed on an Applied Photophysics Pi*-180 stopped flow instrument

(Applied Photophysics, Leatherhead, UK). For unfolding experiments, 3 to 10 μM of protein in buffer (25 mM Tris-HCl, 150 mM NaCl, 1 mM DTT, 0.5 mM EDTA, pH 7.5) was rapidly diluted 1:10 with buffered 2.8 to 8.8 M urea. For refolding experiments, 3 to 10 μM IκBα_{67–206} or 1 to 3 μM IκBα_{67–287} was unfolded in buffered 4 to 5 M urea for at least 30 min and then was rapidly diluted 1:10 with buffered 0 to 3 M urea. Fluorescence was collected perpendicular to the 280-nm emission with a 320-nm cutoff filter over 2 to 200 s. At each urea concentration, 5 to 9 traces were averaged and fit to a sum of exponential decays:

$$\text{Signal} = c + \sum_i A_i \exp(-k_i t)$$

where c is the final fluorescence value, A_i is the amplitudes of the change in fluorescence of each phase, and k_i the observed rate of folding of each phase.

The observed rates were plotted *versus* the final urea concentration to yield chevron plots. The plots were fit to a four-state model^{35,37}:



The function and equation are included in [Supplementary Material](#). Since we have no direct evidence for population of the intermediates, k_{23} and k_{34} were set to 1×10^5 , and m_{23} and m_{34} to 0. The data collected at different temperatures were globally fit with shared m -values. All of the data for the different mutants were also globally fit with shared m -values. Fitting of unfolding and refolding traces as well as chevron plots was performed with Profit (QuantumSoft, Uetikon am See, Switzerland).

Acknowledgements

This work was supported by grant P01-GM071862 and grant R03 TW008232 (to D.U.F.). I.D. acknowledges support from the Molecular Biophysics Training Grant, T32-GM008326.

Supplementary Data

Supplementary data associated with this article can be found, in the online version, at [doi:10.1016/j.jmb.2011.02.021](https://doi.org/10.1016/j.jmb.2011.02.021).

References

- Baeuerle, P. A. & Baltimore, D. (1988). IκB: a specific inhibitor of the NF-κB transcription factor. *Science*, **242**, 540–546.
- Croy, C. H., Bergqvist, S., Huxford, T., Ghosh, G. & Komives, E. A. (2004). Biophysical characterization of the free IκBα ankyrin repeat domain in solution. *Protein Sci.* **13**, 1767–1777.
- Truhlar, S. M., Torpey, J. W. & Komives, E. A. (2006). Regions of IκBα that are critical for its inhibition of NF-κB-DNA interaction fold upon binding to NF-κB. *Proc. Natl Acad. Sci. USA*, **103**, 18951–18956.
- Ferreiro, D. U., Cervantes, C. F., Truhlar, S. M., Cho, S. S., Wolynes, P. G. & Komives, E. A. (2007). Stabilizing IκBα by “consensus” design. *J. Mol. Biol.* **365**, 1201–1216.
- Ferreiro, D. U., Cho, S. S., Komives, E. A. & Wolynes, P. G. (2005). The energy landscape of modular repeat proteins: topology determines folding mechanism in the ankyrin family. *J. Mol. Biol.* **354**, 679–692.
- Ferreiro, D. U. & Wolynes, P. G. (2008). The capillarity picture and the kinetics of one-dimensional protein folding. *Proc. Natl Acad. Sci. USA*, **105**, 9853–9854.
- Werbeck, N. D. & Itzhaki, L. S. (2007). Probing a moving target with a plastic unfolding intermediate of an ankyrin-repeat protein. *Proc. Natl Acad. Sci. USA*, **104**, 7863–7868.
- Bradley, C. M. & Barrick, D. (2002). Limits of cooperativity in a structurally modular protein: response of the Notch ankyrin domain to analogous alanine substitutions in each repeat. *J. Mol. Biol.* **324**, 373–386.
- Bradley, C. M. & Barrick, D. (2006). The notch ankyrin domain folds via a discrete, centralized pathway. *Structure*, **14**, 1303–1312.
- Werbeck, N. D., Rowling, P. J., Chellamuthu, V. R. & Itzhaki, L. S. (2008). Shifting transition states in the unfolding of a large ankyrin repeat protein. *Proc. Natl Acad. Sci. USA*, **105**, 9982–9987.
- Tang, K. S., Fersht, A. R. & Itzhaki, L. S. (2003). Sequential unfolding of ankyrin repeats in tumor suppressor p16. *Structure*, **11**, 67–73.
- Lowe, A. R. & Itzhaki, L. S. (2007). Rational redesign of the folding pathway of a modular protein. *Proc. Natl Acad. Sci. USA*, **104**, 2679–2684.
- Zeeb, M., Rosner, H., Zeslawski, W., Canet, D., Holak, T. A. & Balbach, J. (2002). Protein folding and stability of human CDK inhibitor p19(INK4d). *J. Mol. Biol.* **315**, 447–457.
- Low, C., Weininger, U., Zeeb, M., Zhang, W., Laue, E. D., Schmid, F. X. & Balbach, J. (2007). Folding mechanism of an ankyrin repeat protein: scaffold and active site formation of human CDK inhibitor p19(INK4d). *J. Mol. Biol.* **373**, 219–231.
- Low, C., Weininger, U., Neumann, P., Klepsch, M., Lilie, H., Stubbs, M. T. & Balbach, J. (2008). Structural insights into an equilibrium folding intermediate of an archaeal ankyrin repeat protein. *Proc. Natl Acad. Sci. USA*, **105**, 3779–3784.
- Michaely, P. & Bennett, V. (1992). The ANK repeat: a ubiquitous motif involved in macromolecular recognition. *Trends Cell. Biol.* **2**, 127–129.
- Sedgwick, S. G. & Smerdon, S. J. (1999). The ankyrin repeat: a diversity of interactions on a common structural framework. *Trends Biochem. Sci.* **24**, 311–316.
- Mosavi, L. K., Minor, D. L., Jr. & Peng, Z. Y. (2002). Consensus-derived structural determinants of the ankyrin repeat motif. *Proc. Natl Acad. Sci. USA*, **99**, 16029–16034.
- Binz, H. K., Stumpp, M. T., Forrer, P., Amstutz, P. & Pluckthun, A. (2003). Designing repeat proteins:

- well-expressed, soluble and stable proteins from combinatorial libraries of consensus ankyrin repeat proteins. *J. Mol. Biol.* **332**, 489–503.
20. Kohl, A., Binz, H. K., Forrer, P., Stumpp, M. T., Pluckthun, A. & Grutter, M. G. (2003). Designed to be stable: crystal structure of a consensus ankyrin repeat protein. *Proc. Natl Acad. Sci. USA*, **100**, 1700–1705.
 21. Tripp, K. W. & Barrick, D. (2007). Enhancing the stability and folding rate of a repeat protein through the addition of consensus repeats. *J. Mol. Biol.* **365**, 1187–1200.
 22. Jacobs, M. D. & Harrison, S. C. (1998). Structure of an I κ B α /NF- κ B complex. *Cell*, **95**, 749–758.
 23. DeLano, W. L. (2002). *The PyMOL Molecular Graphics System*. DeLano Scientific, San Carlos, CA, USA.
 24. Barrick, D., Ferreira, D. U. & Komives, E. A. (2008). Folding landscapes of ankyrin repeat proteins: experiments meet theory. *Curr. Opin. Struct. Biol.* **18**, 27–34.
 25. Devi, V. S., Binz, H. K., Stumpp, M. T., Pluckthun, A., Bosshard, H. R. & Jelesarov, I. (2004). Folding of a designed simple ankyrin repeat protein. *Protein Sci.* **13**, 2864–2870.
 26. Wetzel, S. K., Settanni, G., Kenig, M., Binz, H. K. & Pluckthun, A. (2008). Folding and unfolding mechanism of highly stable full-consensus ankyrin repeat proteins. *J. Mol. Biol.* **376**, 241–257.
 27. Interlandi, G., Wetzel, S. K., Settanni, G., Pluckthun, A. & Caffisch, A. (2008). Characterization and further stabilization of designed ankyrin repeat proteins by combining molecular dynamics simulations and experiments. *J. Mol. Biol.* **375**, 837–854.
 28. Guo, Y., Yuan, C., Tian, F., Huang, K., Weghorst, C. M., Tsai, M. D. & Li, J. (2010). Contributions of conserved TPLH tetrapeptides to the conformational stability of ankyrin repeat proteins. *J. Mol. Biol.* **399**, 168–181.
 29. Huxford, T., Huang, D. B., Malek, S. & Ghosh, G. (1998). The crystal structure of the I κ B α /NF- κ B complex reveals mechanisms of NF- κ B inactivation. *Cell*, **95**, 759–770.
 30. Kiefhaber, T., Kohler, H. H. & Schmid, F. X. (1992). Kinetic coupling between protein folding and prolyl isomerization. I. Theoretical models. *J. Mol. Biol.* **224**, 217–229.
 31. Pappenberger, G., Aygun, H., Engels, J. W., Reimer, U., Fischer, G. & Kiefhaber, T. (2001). Nonprolyl *cis* peptide bonds in unfolded proteins cause complex folding kinetics. *Nat. Struct. Biol.* **8**, 452–458.
 32. Oliveberg, M. (2001). Characterisation of the transition states for protein folding: towards a new level of mechanistic detail in protein engineering analysis. *Curr. Opin. Struct. Biol.* **11**, 94–100.
 33. Mello, C. C., Bradley, C. M., Tripp, K. W. & Barrick, D. (2005). Experimental characterization of the folding kinetics of the notch ankyrin domain. *J. Mol. Biol.* **352**, 266–281.
 34. Lowe, A. R. & Itzhaki, L. S. (2007). Biophysical characterisation of the small ankyrin repeat protein myotrophin. *J. Mol. Biol.* **365**, 1245–1255.
 35. Bachmann, A. & Kiefhaber, T. (2001). Apparent two-state tandemistat folding is a sequential process along a defined route. *J. Mol. Biol.* **306**, 375–386.
 36. Bachmann, A. & Kiefhaber, T. (2005). Protocols—analytical solutions of three-state protein folding models. In *Protein Folding Handbook: Part 1* (Buchner, J. & Kiefhaber, T., eds), Vol. 1, pp. 402–406. Wiley-VCH Verlag GmbH & Co. KGaA, Weinheim.
 37. Sanchez, I. E. & Kiefhaber, T. (2003). Evidence for sequential barriers and obligatory intermediates in apparent two-state protein folding. *J. Mol. Biol.* **325**, 367–376.
 38. Fersht, A. R., Matouschek, A. & Serrano, L. (1992). The folding of an enzyme. I. Theory of protein engineering analysis of stability and pathway of protein folding. *J. Mol. Biol.* **224**, 771–782.
 39. Itzhaki, L. S., Otzen, D. E. & Fersht, A. R. (1995). The structure of the transition state for folding of chymotrypsin inhibitor 2 analysed by protein engineering methods: evidence for a nucleation–condensation mechanism for protein folding. *J. Mol. Biol.* **254**, 260–288.
 40. Tripp, K. W. & Barrick, D. (2004). The tolerance of a modular protein to duplication and deletion of internal repeats. *J. Mol. Biol.* **344**, 169–178.
 41. Papworth, C., Bauer, J. C., Braman, J. & Wright, D. A. (1996). Site-directed mutagenesis in one day with >80% efficiency. *Strategies*, **8**, 3–4.
 42. Truhlar, S. M., Mathes, E., Cervantes, C. F., Ghosh, G. & Komives, E. A. (2008). Pre-folding I κ B α alters control of NF- κ B signaling. *J. Mol. Biol.* **380**, 67–82.
 43. Street, T. O., Courtemanche, N. & Barrick, D. (2008). Protein folding and stability using denaturants. *Methods Cell. Biol.* **84**, 295–325.
 44. Pace, C. N. (1986). Determination and analysis of urea and guanidine hydrochloride denaturation curves. *Methods Enzymol.* **131**, 266–280.